Chinese Chemical Letters 33 (2022) 893–897

Contents lists available at ScienceDirect

Chinese Chemical Letters

journal homepage: www.elsevier.com/locate/cclet

The role of Si coordination structures in the catalytic properties and durability of Cu-SAPO-34 as NH_3-SCR catalyst for NO_x reduction

Zhen Chen[1], Ce Bian[1], Chi Fan, Tao Li*

Key Laboratory of Material Chemistry for Energy Conversion and Storage, Ministry of Education, Hubei Key Laboratory of Material Chemistry and Service Failure, School of Chemistry and Chemical Engineering, Huazhong University of Science and Technology, Wuhan 430074, China

ARTICLE INFO

Article history:
Received 19 January 2021
Revised 14 May 2021
Accepted 25 June 2021
Available online 2 July 2021

Keywords:
NO_x
NH_3-SCR
Cu-SAPO-34
Si coordination structure
Hydrothermal stability

ABSTRACT

Si coordination structures have been proven to greatly influence the ammonia-selective catalytic reduction (NH_3-SCR) catalytic properties and the hydrothermal stability of Cu-based silicoaluminophosphate-form catalysts. However, the role of various Si coordination structures in the NH_3-SCR reaction over Cu-SAPO-34 catalyst remains unknown. Herein, a batch of Cu-SAPO-34 samples with various Si contents was synthesized *via* a one-pot method to study the role of Si coordination structures in the NH_3-SCR catalytic properties and hydrothermal stability. Cu/34–2 with the highest proportion of Si(xOAl) (x = 1~3) structures exhibits remarkable durability with 90% NO reduction efficiency within 200~450 °C even after a hydrothermal aging treatment at 850 °C. In contrast, Cu/34–1 and Cu/34–4 with the highest proportions of Si(4OAl) and Si(0OAl) structures, respectively, are significantly deactivated by the same hydrothermal treatment. To better understand this phenomenon, the relationship between the Si coordination structures and SCR performance is established using characterization techniques and kinetics measurements. Results reveal that a high content of Si(4OAl) and Si(0OAl) is detrimental to the hydrothermal stability of Cu-SAPO-34 catalyst. However, Si(xOAl) (x = 1~3) structures are conducive to the stabilization of isolated Cu^{2+}, thus enhancing the stability to severe hydrothermal treatment.

Nitric oxide (NO_x) from fossil fuel combustion poses a great threat to human health, particularly in developing countries. Among them, NO_x emissions from diesel vehicle exhaust share a large portion of the overall NO_x pollution [1,2]. Copper-based chabazite (CHA) zeolites (including SSZ-13 and SAPO-34) have been comprehensively investigated as ammonia-selective catalytic reduction (NH_3-SCR) catalysts for NO_x elimination in diesel engine vehicles due to their remarkable performance over a broad operating temperature window, high N_2 selectivity, superior hydrothermal stability and excellent hydrocarbon resistance [3,4]. Cu-SAPO-34 is one of the most attractive SCR catalysts because of its superior NH_3-SCR activity and hydrothermal stability, while being inexpensive [5]. In particular, Epling *et al.* [6] reported that Cu-SAPO-34 is more robust than the Cu-SSZ-13 catalyst when undergoing the same hydrothermal treatment. Besides, the morphology of the catalyst plays an important role in the catalytic activity [7-11]. Our previous work [12] also prepared a submicron Cu-SAPO-34 catalyst with excellent NH_3-SCR activity and hydrothermal stability (90% NO conversion within 225–550 °C after hydrothermal treatment at 800 °C) by a one-pot method.

Currently, research on Cu-SAPO-34 for NH_3-SCR applications is mainly focused on the following three topics: improvements in its catalytic activity and hydrothermal stability, studies on the distribution and evolution of Cu species, and the roles of acidity and function of different acid sites during the NH_3-SCR reaction [13-17]. However, all the above important factors for the Cu-SAPO-34 catalyst are ultimately affected by the Si coordination structures in SAPO-34 zeolite. In general, the various Si coordination structures in SAPO-34 have distinct acid properties. Thus, the Si distribution can determine the acid strength and content in SAPO-34, resulting in a distinct Cu distribution and affecting the catalytic activity and hydrothermal stability of Cu-SAPO-34. Furthermore, the different acid sites have distinct functions in the NH_3-SCR reaction [17]. Therefore, it can be deduced that the variety of Si coordination structures have distinct roles in the NH_3-SCR reaction. Many studies [18-21] agree that the presence of numerous Si islands (Si(0OAl)) in the Cu-SAPO-n zeolite is detrimental to the NH_3-SCR reaction. Si islands cannot generate acid sites because these islands cannot provide an acid center for the reaction. In addition, Si islands without acid sites do not work efficiently

* Corresponding author.
E-mail address: taoli@hust.edu.cn (T. Li).
[1] These authors contributed equally to this work.

https://doi.org/10.1016/j.cclet.2021.06.071
1001-8417/

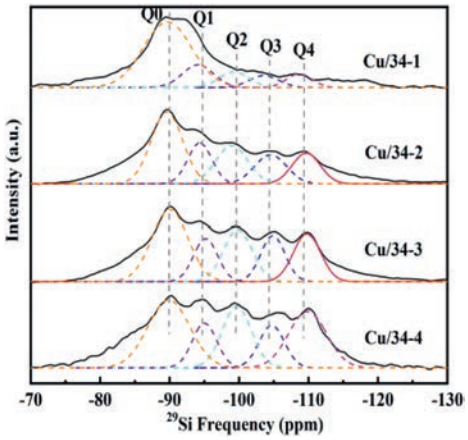

Fig. 1. Solid-state ^{29}Si MAS NMR of Cu-SAPO-34 catalysts with different Si content.

in stabilizing the extraframework Cu^{2+} ions [21]. Nevertheless, the roles of the other Si coordination structures in the NH_3-SCR reaction are still unclear. Hence, it is very interesting to investigate the role of distinct Si coordination structures in the SCR performance of Cu-SAPO-34 catalyst because the Si coordination structures may contribute to the synthesis of a highly efficient and robust metal modified zeolite catalyst. In this study, four Cu-SAPO-34 catalysts with different contents of Si(xOAl) (x = 0–4) coordination structures are synthesized by tuning the Si content in the starting gels to explore the role of Si coordination structures in the NH_3-SCR reaction. The synthesis procedure of Cu-SAPO-34 with different Si contents and experimental methods are provided in the Supporting information in detail.

The chemical compositions of Cu/34–1~Cu/34–4 are listed in Table S1 (Supporting information). The [Si/(Al + P)] ratios of these four samples analyzed by X-ray fluorescence (XRF) are 0.144, 0.210, 0.260 and 0.333. This result indicates that the Si content in SAPO-34 can be tuned by the addition of Si in synthetic gels. The Cu loadings in Cu-34–1~Cu-34–4 are equivalent to 4.1%, as measured by inductively coupled plasma-atomic emission spectrometry (ICP-AES). The scanning electron microscopy (SEM) images (Figs. S1 and S2 in supporting information) clearly show typical cubic crystals of these Cu-SAPO-34 samples with crystal sizes distributed in the 0.5~1.0 μm range. After hydrothermal aging, the crystalline structure of each sample has a different degree of damage. Among them, the cubical morphology of Cu/34–2-A800 and Cu/34–2-A850 maintains the best. The ^{29}Si magic angle spinning nuclear magnetic resonance (^{29}Si MAS NMR) spectra of the Cu-SAPO-34 catalysts in Fig. 1 present multiple characteristic peaks at −90.5, −94.3, −99.5, −105.3 and −110.1 ppm, which are attributed to the Q0 (Si(4OAl)), Q1 (Si(3OAl)), Q2 (Si(2OAl)), Q3 (Si(1OAl)) and Q4 (Si(0OAl)) coordination structures, respectively [22]. Table S2 (Supporting information) presents the relative contents of different Si coordination structures in the Cu-SAPO-34 samples based on Gaussian deconvolution of the ^{29}Si NMR spectra. Clearly, the Si distribution is vitally influenced by the Si content in the Cu-SAPO-34 catalysts. The relative contents of the Si(4OAl) structure (isolated Si) in Cu/34–1~Cu/34–4 are 63.2%, 36.1%, 34.5% and 31.9%, respectively, and this value decreases with an increasing Si content, as shown in Fig. S3a (Supporting information). The relative contents of Si(0OAl) structure (Si islands) in Cu/34–1~Cu/34–4 are 6.8%, 13.7%, 17.3% and 23.9%, respectively, which increases with Si content raising, as shown in Fig S3b (Supporting information). The relative content of Si(xOAl) (x = 1~3) structures in Cu/34–1~Cu/34–4 is 30.0%, 50.2%, 48.2% and 44.2%, respectively, first showing an increase and then decreasing with an increasing Si content before reaching a maximum in Cu/34–2, as shown in Fig. S3c (Supporting information). On the basis of the above results, the Si content and coordination structures in SAPO-34 can be regulated by the addition of the silicon source in the initial synthesis gels. The XRD patterns of these fresh Cu-SAPO-34 samples are shown in Fig. S4 (Supporting information), and each sample reveals the typical CHA structure without impurities [12,23]. Weak peaks related to CuO phases (2θ = 35.5° and 38.6°, marked with a ♥) are also observed over the fresh samples, which is probably due to the relatively high Cu loadings. The intensity of the CuO peaks decreases as the Si content increases, and the CuO species can hardly be detected in Cu/34–4. A possible explanation is that the SAPO-34 zeolite with a higher Si content can provide more exchange sites for Cu loading to form isolated Cu^{2+} ions. Upon hydrothermal treatment at 800 °C for 12 h, the relative crystallinity of each sample evidently decreases while maintaining the typical CHA structure, as shown in Fig. S4b. Among them, the intensity of CHA peaks over Cu/34–2-A800 is the highest, indicating that it is the most stable during hydrothermal treatment. Furthermore, the intensity of the CuO peaks is weakened for all catalysts aged at 800 °C due to the redistribution of CuO. When a harsher hydrothermal treatment (aging at 850 °C for 12 h) is performed over the as-prepared catalysts, the transformation of the CHA zeolite into the tridymite dense phase (2θ = 21.5°, marked with a ♣) is detected over all samples, indicating the desilication of Cu-SAPO-34 when aging at 850 °C [24,25]. Comparatively speaking, Cu/34–2 has the lowest observed desilication, suggesting that it is more stable toward severe conditions than the other catalysts, as described in Fig. S4c.

Ammonia-temperature programmed desorption (NH_3-TPD) measurements were carried out to quantify the acidity of these as-prepared catalysts, as shown in Fig. 2. All these samples contain three NH_3 desorption peaks, named A, B and C, which are attributed to NH_3 desorption from weak, moderate and strong acid sites, respectively [12,26,27]. The quantitative acidity results are is listed in Table S3 (Supporting information). The total acid contents of Cu/34–1~Cu/34–4 are 0.484, 0.664, 0.724 and 0.867 mmol/g, respectively, showing an increase with an increasing Si content, as shown in Table S3 (Supporting information). This result is in line with the variation trend of the total content of Si(xOAl) (x = 1~4) structures in the Cu-SAPO-34 catalysts. This result is because most of the acid sites originate from protons, which compensate for the unbalanced electric charges coming from the incorporation of Si into the neutral framework of the AlPO zeolites [28-30]. Fig. S5a (Supporting information) shows a linear relationship between the acid content and the [Si/(Al + P)] ratio in the fresh Cu-SAPO-34 catalysts. Note that the acid strength of the prepared Cu-SAPO-34 catalysts ranks in the order of Cu/34–2 ≈ Cu/34–3 > Cu/34–4 > Cu/34–1. Considering that the relative acid strength of the distinct Si coordination structures presents the following sequence: Si(1OAl) > Si(2OAl) > Si(3OAl) > Si(4OAl) > Si(0OAl) [28], the higher content of Si(xOAl) (x = 1~3) structures results in the stronger acidity of the Cu-SAPO-34 catalyst. After the hydrothermal aging treatment at 800 °C, most of the acid sites are retained in the Cu-SAPO-34 catalysts, and the acid content decreases by 38%, 23%, 36% and 31% for Cu/34–1~Cu/34–4, respectively. When the hydrothermal aging temperature is further increased to 850 °C, the acid content of these catalysts (Cu/34–1~Cu/34–4) decreases by 64%, 49%, 64% and 78%, respectively, indicating that most of the acid sites disappear under harsher conditions. Note that the acid contents of catalysts aged at 850 °C present peak curves with an increasing [Si/(Al + P)] ratio and reach a maximum with Cu/34–2-A850, as shown in Fig. S5c (Supporting information). The samples rank in the order of Cu/34–2-A850 > Cu/34–3-A850 > Cu/34–4-A850 > Cu/34–1-A850. From the NH_3-TPD results, it is reasonable to conclude that the Cu-SAPO-34 catalysts can withstand the hydrothermal treatment at 800 °C for 12 h, but they lose most of their acid sites during aging at 850 °C. Among them,

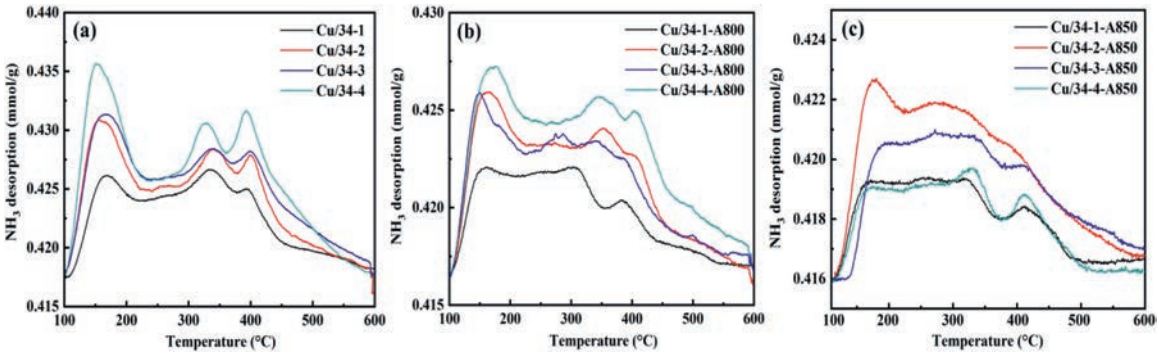

Fig. 2. NH_3-TPD over fresh and hydrothermal aged Cu-SAPO-34 samples: (a) Fresh catalysts, (b) catalysts after hydrothermal aged at 800 °C for 12 h, (c) catalysts after hydrothermal aged at 850 °C for 12 h.

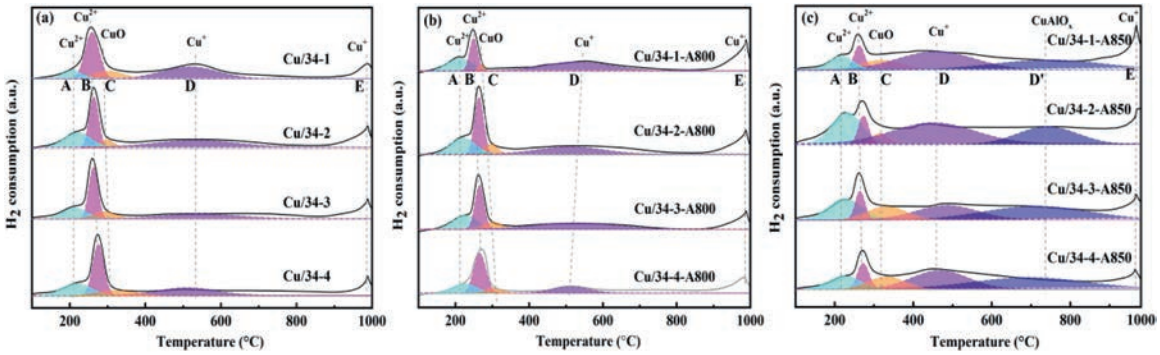

Fig. 3. H_2-TPR patterns of the fresh and hydrothermal aged Cu-SAPO-34 catalysts: (a) Fresh catalysts, (b) catalysts after hydrothermal aged at 800 °C for 12 h, (c) catalysts after hydrothermal aged at 850 °C for 12 h.

Cu/34–2 exhibits the best hydrothermal stability and maintains the highest number of acid sites, whether treated at 800 °C or 850 °C.

H_2-TPR measurements over fresh and aged Cu-SAPO-34 catalysts were performed to explore the effect of Si coordination structures on the Cu distribution, as shown in Fig. 3. The patterns of all the fresh and aged catalysts can be deconvoluted into five peaks (Peaks A~E) by the Gaussian method. Peaks A (~210 °C) and B (~260 °C) are attributed to the reduction of isolated Cu^{2+} ions located at different sites (in the CHA cage and D6Rs, respectively). Peak C (~300 °C) is related to the reduction of CuO to Cu^0. Peaks D (~530 °C) and E (~980 °C) are assigned to the reduction of Cu^+ ions to Cu^0 [12,31-33]. Specifically, a new peak D' (~740 °C) is observed for the catalysts aged at 850 °C, corresponding to the reduction of $CuAlO_x$ nanoparticles to Cu^0 due to the dealumination of the zeolite framework [34,35]. The H_2-TPR curves of the fresh catalysts are similar, indicating a comparable Cu distribution. Moreover, isolated Cu^{2+} is the predominant Cu species in the fresh catalysts. The content of Cu^+ ions (peak D) in Cu/34–1 is higher than that in the other fresh catalysts.

Regarding the catalysts after the hydrothermal treatment at 800 °C for 12 h, the H_2-TPR curves have no large changes compared with those of the fresh catalysts except for the weakening of peak C, which is related to CuO. This result agrees well with the XRD results. This phenomenon can be attributed to the redistribution of CuO during hydrothermal treatment. According to Fig. 3b, the amount of isolated Cu^{2+} ions in the aged catalysts ranks in the following order: Cu/34–2-A800 > Cu/34–3-A800 > Cu/34–4-A800 > Cu/34–1-A800. When more severe aging conditions (850 °C and 12 h) are adopted, the amount of isolated Cu^{2+} ions (Peaks A and B) decreases, while the amount of CuO (Peak C) and Cu^+ ions (Peak D) increases. Additionally, the number of Cu^{2+} ions located in the CHA cage (Peak A) increases. More importantly, a new peak representative of $CuAlO_x$ nanoparticles centered at approximately 740 °C appears. At high temperatures and under moist conditions, the zeolite framework is unstable and can be damaged, as proven by the appearance of the tridymite dense phase observed in the XRD results of the aged catalysts in Fig. S4c. The desilication and dealumination of the SAPO-34 support lead to the formation of a dense tridymite phase and extra-framework aluminum species, respectively. Thereafter, the interaction of isolated Cu^{2+} ions and extraframework aluminum species results in the generation of $CuAlO_x$ species [35]. The increased amount of CuO, Cu^+ and $CuAlO_x$ species leads to the decrease in the number of isolated Cu^{2+} ions. After hydrothermal treatment at 850 °C for 12 h, the amount of the isolated Cu^{2+} ions in these aged catalysts ranks in the following order: Cu/34–2-A850 > Cu/34–3-A850 > Cu/34–1-A850 > Cu/34–4-A850, as shown in Fig. 3c. This result suggests that the isolated Cu^{2+} ions in Cu/34–1 and Cu/34–4 are not as stable as those in Cu/34–2 and Cu/34–3 during a severe aging treatment. This observation can be attributed that Cu/34–2 and Cu/34–3 containing more strong acid sites generated by Si(xOAl) (x = 1~3) structures, which have a better stabilization effect on Cu^{2+} ions [21,36].

To study the effect of Si coordination structures on the SCR catalytic activity and hydrothermal stability of Cu-SAPO-34, the NO conversions of fresh and aged Cu-SAPO-34 catalysts with distinct Si contents were measured. Fig. 4a shows the NO conversions of the fresh Cu-SAPO-34 catalysts within 175–575 °C, and all these catalysts exhibit excellent activity with a 90% NO conversion within 200–550 °C. Furthermore, the NO conversion increases with an increasing Si content over the whole temperature range. This result indicates that the NO conversions are related to the acidity of the fresh catalysts. Moreover, more acid sites can provide more exchange sites for Cu loading. Hence, the amount of isolated Cu^{2+} ions, which are the active sites for the NH_3-SCR reaction, increases

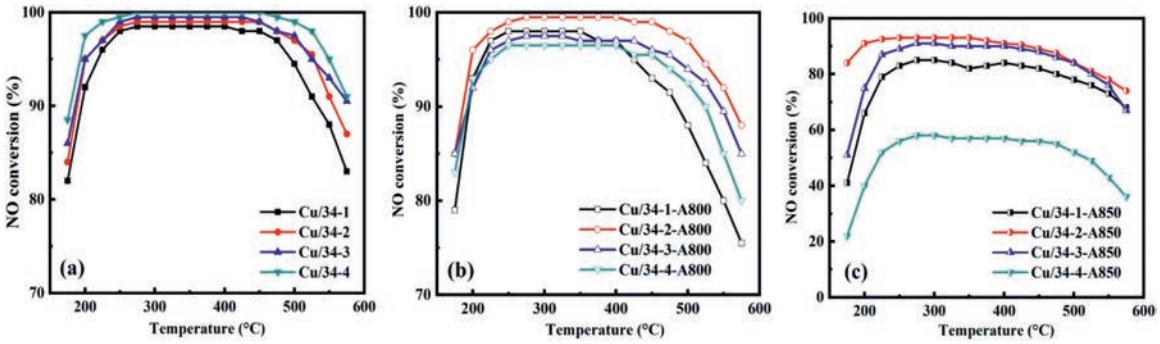

Fig. 4. Catalytic activity for the SCR of NO reaction of Cu-SAPO-34 catalysts: (a) fresh catalysts; (b) catalysts after hydrothermal aged at 800 °C for 12 h; (c) catalysts after hydrothermal aged at 850 °C for 12 h.

with an increasing Si content as verified by H_2-TPR. Based on the above results, the relationships among the Si content, Si coordination structures, acidity, Cu distribution and catalytic activity over the fresh Cu-SAPO-34 catalysts can be summarized as follows. (1) A higher Si content results in more Si(xOAl) (x = 1~4) structures in the SAPO-34 support, which can generate strong acid sites by proton charge compensation. Therefore, higher Si content leads to more acid sites. (2) The acid sites can act as exchange sites for Cu loading. Hence, more acid sites result in a higher content of isolated Cu^{2+} ions in the Cu-SAPO-34 catalysts. 3) As is well known, the acidic site and isolated Cu^{2+} ions act synergistically as reaction sites in the NH_3-SCR reaction [17,37-39]. Therefore, a higher Si content leads to better NO conversion over fresh Cu-SAPO-34 catalysts. This result agrees well with studies reported by Shen *et al.* in which the SCR low-temperature activity is related to the acid site density [40].

After the hydrothermal treatment at 800 °C for 12 h, the discrepancies in the NO conversion among these catalysts become more apparent, as shown in Fig. 4b. The NO conversions of the aged catalysts above 400 °C and below 200 °C decrease in the order of Cu/34–2-A800 > Cu/34–3-A800 > Cu/34–4-A800 > Cu/34–1-A800. The NO conversions within 200–400 °C rank in the order of Cu/34–2-A800 > Cu/34–1-A800 > Cu/34–3-A800 > Cu/34–4-A800. After the more severe hydrothermal treatment at 850 °C for 12 h, the catalytic activities of all catalysts evidently decrease, as shown in Fig. 4c. However, Cu/34–2-A850 still maintains excellent activity with 90% NO conversion within 200~450 °C, indicating its remarkable hydrothermal stability. The NO conversions of the aged catalysts over the whole temperature range rank in the order of Cu/34–2-A850 > Cu/34–3-A850 > Cu/34–1-A850 > Cu/34–4-A850. Specifically, the NO conversion over Cu/34–1-A850~Cu/34–4-A850 at 175 °C is 41%, 84%, 51% and 22%, respectively. At 400 °C, the NO conversion over Cu/34–1-A850~Cu/34–4-A850 is 91%, 90%, 83% and 57%, respectively. This result indicates that the hydrothermal stability of Cu-SAPO-34 is significantly influenced by the Si content. Based on the XRD, ^{29}Si NMR, NH_3-TPD, H_2-TPR and catalytic activity results, the relationship between the Si coordination structures and the hydrothermal stability of Cu-SAPO-34 catalysts can be summarized as follows. (1) After the hydrothermal treatments at 800 °C and 850 °C, the sharply decreased number of acid sites and isolated Cu^{2+} ions in Cu/34–1 lead to a decline in catalytic activity. This result indicates that Cu-SAPO-34 with a low Si content and predominant Si(4OAl) structure shows poor hydrothermal stability. (2) On the other hand, the catalytic activity, acidity and content of Cu^{2+} ions in Cu/34–4-A800 and Cu/34–4-A850 also decrease significantly, suggesting that Si islands (Si(0OAl)) are also not stable during a severe hydrothermal treatment. Because Si islands cannot produce acid sites, they are not capable of providing anchored sites for protecting the extraframework Cu^{2+} ions in the Cu-SAPO-34 catalyst during hydrothermal treatment. Furthermore, the relative crystallinity of Cu/34–4 drops sharply after hydrothermal treatment. Although the content of Si(xOAl) (x = 1~3) structures in Cu/34–4 is only 6% lower than that in Cu/34–2, the activity of Cu/34–4-A850 is the worst among the aged catalysts. This result is probably due to Cu/34–4 having the highest content of Si islands (23.9%). These Si islands are unstable and vulnerable to desiliconization during hydrothermal treatment, leading to the collapse of the zeolite framework. (3) Cu/34–2 is the most hydrothermally stable among the catalysts. After the hydrothermal treatment at 850 °C, the variation trend of NO conversion is basically consistent with the variation in the content of acidity, isolated Cu^{2+} ions and Si(xOAl) (x = 1~3) structures in the catalysts. This result indicates that the Si(xOAl) (x = 1~3) structures play an important role in the acidity, Cu distribution and hydrothermal stability of the Cu-SAPO-34 catalyst. This finding can be attributed to the following reasons: the distinct Si coordination structures exhibit different acid strengths as follows: Si(0OAl) < Si(4OAl) < Si(3OAl) < Si(2OAl) < Si(1OAl). A higher content of Si(xOAl) (x = 1~3) structures can produce more strong acid sites in the SAPO-34 zeolite. Our previous work has proven that the strong acid sites produced by Si(xOAl) (x = 1~3) structures are conducive to the stabilization of isolated Cu^{2+} ions in Cu-SAPO-18 catalysts during hydrothermal treatment [21]. Furthermore, Valange *et al.* [46] also verified that Cu species could be better stabilized in ZSM-5 zeolite with strong acidity. Hence, it is reasonable to conclude that Si(xOAl) (x = 1~3) structures are also conducive to the improvement in the hydrothermal stability of Cu-SAPO-34 catalyst. This is also demonstrated not only by the catalytic activity of aged catalysts but also by the changes of the acid content and active isolated Cu^{2+} ions in the catalysts. To evaluate the stability of the Cu/34–2 catalyst, the NO conversions over Cu/34–2 at 400 °C are tested during 16 h, as shown in Fig. S6 (Supporting information). The NO conversion maintains above 98% even after 16 h reaction. It shows the excellent stability of Cu/34–2, which is consistent with the excellent hydrothermal stability after 850 °C hydrothermal aging treatment.

To further study the effect of the Si coordination structures on the SCR reaction mechanism, NH_3-SCR kinetics analysis was performed over the Cu-SAPO-34 catalysts at low temperatures. The NH_3-SCR reaction rates over the Cu-SAPO-34 catalysts within 100~200 °C were calculated by Eq. S2 (Supporting information), where the NO conversion is less than 20%. Arrhenius plots of the SCR reaction rate over the Cu-SAPO-34 catalysts with different [Si/(Al + P)] ratios and Si coordination structures are shown in Fig. S7 (Supporting information). The apparent activation energy (E_a) of these Cu-SAPO-34 catalysts for the NH_3-SCR reaction is 38.4 ± 1.2 kJ/mol, which is close to the E_a value (37.49 ± 2.5 kJ/mol) measured by Shen *et al.* [28]. The similar E_a values of these Cu-SAPO-34 catalysts suggest that the Si content

and Si coordination structures do not influence the NH_3-SCR reaction mechanism. There are two explanations to be considered. (1) The Si content and Si coordination structures mainly affect the acid content and strength of SAPO-34 [19,21], and the acidity can influence NH_3 storage and the relative amount of Cu^{2+} and CuO species. (2) Previous works have proven that the content of acid sites and Cu^{2+} ions does not change the NH_3-SCR reaction mechanism [40,41].

In summary, four Cu-SAPO-34 catalysts with different Si distributions are synthesized *via* a one-pot method to study the role of Si coordination structures in the catalytic properties of Cu-SAPO-34 catalysts. An ultrastable Cu-SAPO-34 catalyst with a suitable Si content ([Si/Al + P] = 0.210) and a high content of Si(xOAl) (x = 1~3) structures (50.2%) is obtained, showing 90% NO conversion within 200~450 °C even after hydrothermal treatment at 850 °C. The structure-performance relationships among the Si coordination structures, acidity, Cu distribution and SCR performance are established by obtaining the XRD, NMR, NH_3-TPD and H_2-TPR results, which can be summarized as follows. (1) The Si coordination environment in Cu-SAPO-34 can be adjusted by the addition of a Si precursor. When more Si precursors are added to the initial gels, more Si islands (Si(0OAl)) and less isolated Si (Si(4OAl)) are generated in Cu-SAPO-34. (2) Compared with weak acid sites, strong acid sites are more conducive to the stability of isolated Cu^{2+} ions. (3) High content of isolated Si (Si(4OAl)) and Si islands (Si(0OAl)) are not good for the hydrothermal stability of the Cu-SAPO-34 catalyst. However, the strong acid sites generated by Si(xOAl) (x = 1~3) structures are conducive to the stabilization of isolated Cu^{2+} ions, thus enhancing the hydrothermal stability of the Cu-SAPO-34 catalyst. This work provides new insight into the effect of Si coordination structures on the performance of transition metal modified zeolite catalysts, which will be beneficial for the design and synthesis of high-performance and robust catalysts.

Declaration of competing interest

The authors declared that they have no conflicts of interest to this work.

Acknowledgments

The authors gratefully acknowledge financial support from the National Natural Science Foundation of China (No. 52000084) and the China Postdoctoral Science Foundation (No. 2019M662630). The authors also thank for the characterizations offered by the Analytical and Testing Center, Huazhong University of Science and Technology, Wuhan, China.

Supplementary materials

Supplementary material associated with this article can be found, in the online version, at doi:10.1016/j.cclet.2021.06.071.

References

[1] Y. Tan, P. Henderick, S. Yoon, et al., Environ. Sci. Technol. 53 (2019) 5504–5511.
[2] J. Du, X. Shi, Y. Shan, et al., Environ. Sci. Technol. 54 (2020) 7870–7878.
[3] A.M. Beale, F. Gao, I. Lezcano-Gonzalez, C.H.F. Peden, J. Szanyi, Chem. Soc. Rev. 44 (2015) 7371–7405.
[4] S. Zhang, L. Pang, Z. Chen, et al., Appl. Catal. A 607 (2020) 117855.
[5] L. Sun, M. Yang, Y. Cao, et al., Chin. J. Catal. 41 (2020) 1410–1420.
[6] D. Wang, Y. Jangjou, Y. Liu, et al., Appl. Catal. B 165 (2015) 438–445.
[7] L. Wang, J. Wan, Y. Zhao, N. Yang, D. Wang, J. Am. Chem. Soc. 141 (2019) 2238–2241.
[8] F. You, J. Wan, J. Qi, et al., Angew. Chem., Int. Ed. 132 (2020) 731–734.
[9] H. Wang, J. Qi, N. Yang, et al., Angew. Chem. Int. Ed. 59 (2020) 19691–19695.
[10] H. Wang, D. Mao, J. Qi, et al., Adv. Funct. Mater. 29 (2019) 1806588.
[11] Y. Wei, J. Wan, N. Yang, et al., Natl. Sci. Rev. 7 (2020) 1638–1646.
[12] Z. Chen, C. Fan, L. Pang, et al., Appl. Surf. Sci. 448 (2018) 671–680.
[13] D. Zhang, R.T. Yang, Appl. Catal. A 543 (2017) 247–256.
[14] C. Niu, X. Shi, K. Liu, et al., Catal. Commun. 81 (2016) 20–23.
[15] L. Wang, J.R. Gaudet, W. Li, D. Weng, J. Catal. 306 (2013) 68–77.
[16] X. Liu, X. Wu, D. Weng, Z. Si, R. Ran, Catal. Today 281 (2017) 596–604.
[17] L. Wang, W. Li, S.J. Schmieg, D. Weng, J. Catal. 324 (2015) 98–106.
[18] R. Martínez-Franco, M. Moliner, C. Franch, A. Kustov, A. Corma, Appl. Catal. B 127 (2012) 273–280.
[19] J. Wang, T. Yu, X. Wang, et al., Appl. Catal. B 127 (2012) 137–147.
[20] R. Martínez-Franco, M. Moliner, A. Corma, J. Catal. 319 (2014) 36–43.
[21] Z. Chen, C. Fan, L. Pang, et al., Chem. Eng. J. 348 (2018) 608–617.
[22] W. Shen, X. Li, Y. Wei, et al., Micropor. Mesopor. Mater. 158 (2012) 19–25.
[23] M. Xu, J. Wang, T. Yu, J. Wang, M. Shen, Appl. Catal. B 220 (2018) 161–170.
[24] R. Martínez-Franco, M. Moliner, P. Concepcion, J.R. Thogersen, A. Corma, J. Catal. 314 (2014) 73–82.
[25] D. Fan, J. Wang, T. Yu, et al., Chem. Eng. Sci. 176 (2018) 285–293.
[26] R. Li, P. Wang, S. Ma, et al., Chem. Eng. J. 379 (2020) 122376.
[27] Y. Wan, G. Yang, J. Xiang, et al., Dalton Trans. 49 (2020) 764–773.
[28] T. Yu, D. Fan, T. Hao, et al., Chem. Eng. J. 243 (2014) 159–168.
[29] X. Shen, Y. Du, J. Ding, et al., ChemCatChem 12 (2020) 4904–4910.
[30] G. Pétaud, F. Gaillard, M. Tayakout, S. Gil, A. Giroir-Fendler, ChemCatChem 12 (2020) 2807–2822.
[31] Y. Ma, X. Wu, L. Liu, et al., Appl. Catal. B 278 (2020) 119306.
[32] J. Cheng, S. Han, Q. Ye, et al., Res. Chem. Intermed. 45 (2019) 2023–2044.
[33] M. Urrutxua, B. Pereda-Ayo, U. De-La-Torre, J.R. González-Velasco, ACS Omega 4 (2019) 14699–14713.
[34] U. Deka, I. Lezcano-Gonzalez, S.J. Warrender, et al., Microporous Mesoporous Mater 166 (2013) 144–152.
[35] C. Wang, W. Yan, Z. Wang, et al., Catal. Today 355 (2020) 482–492.
[36] S. Valange, Z. Gabelica, M. Abdellaoui, J. Clacens, J. Barrault, Microporous Mesoporous Mater. 30 (1999) 177–185.
[37] L. Xie, F. Liu, L. Ren, et al., Environ. Sci. Technol. 48 (2013) 566–572.
[38] Y. Ma, X. Wu, S. Cheng, et al., Appl. Catal. A 602 (2020) 117650.
[39] G. Pétaud, S. Gil, A. Giroir-Fendler, M. Tayakout-Fayolle, Ind. Eng. Chem. Res. 59 (2020) 15848–15864.
[40] T. Yu, J. Wang, M. Shen, W. Li, Catal. Sci. Technol. 3 (2013) 3234–3241.
[41] D. Wang, L. Zhang, J. Li, K. Kamasamudram, W.S. Epling, Catal. Today 231 (2014) 64–74.